Inorganic Chemistry

Article

pubs.acs.org/IC

Stereoselective Postassembly CH Oxidation of Self-Assembled Metal–Ligand Cage Complexes

Lauren R. Holloway, Paul M. Bogie, Yana Lyon, Ryan R. Julian, and Richard J. Hooley*

Department of Chemistry, University of California—Riverside, Riverside, California 92521, United States

Supporting Information

ABSTRACT: Self-assembled Fe-iminopyridine cage complexes containing doubly benzylic methylene units such as fluorene and xanthene can be selectively oxidized at the ligand backbone with ^{t}BuOOH, with no competitive oxidation observed at the metal centers. The self-assembled cage structure controls the reaction outcome, yielding oxidation products that are favored by the assembly, not by the reactants or functional groups. Whereas uncomplexed xanthene and fluorene control ligands are solely oxidized to the ketone equivalents with ^{t}BuOOH, the unfavorability of the self-assembled ketone cages forces the reaction to form the ^{t}butyl peroxide and alcohol-containing oxidation products, respectively. In addition, the oxidation is diastereoselective, with only single isomers of the cage assemblies formed, despite the presence of as many as 10 stereocenters in the final product. The self-assembled structures exploit self-complementary hydrogen bonding and geometrical constraints to direct the postassembly reactions to outcomes not observed in free solution. This selectivity is reminiscent of the fine control of post-translational modification seen in biomacromolecules.

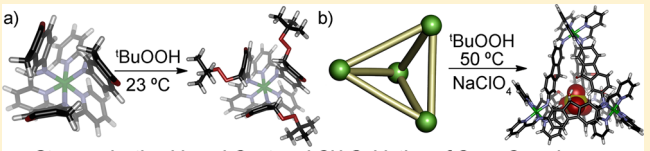

Stereoselective Ligand-Centered CH Oxidation of Cage Complexes

INTRODUCTION

One of the hallmarks of cellular regulation is the ability to effect structural and functional changes in proteins upon post-translational modification.[1] Small changes in backbone structure, such as the addition of phosphate groups to serine residues, can cause extensive changes to the macroscopic structure and, concomitantly, the protein function.[2] This behavior is unique to proteins and relies on the structural complexity of the biomacromolecule.

Of course, there are also a number of small molecule systems that mimic proteinic behavior. Self-assembled metal–ligand cage complexes display many characteristics of enzymes, in that they can accelerate[3] and catalyze[4] reactions of bound substrates, as well as stabilizing reactive species[5] and favoring reaction outcomes that are "impossible" in free solution.[6] Less well-explored is the effect of self-assembly and self-folding on the outcome of reactions on the structural framework of the cage. In contrast with the wealth of literature on metal–organic framework modification,[7] postassembly modification (PAM) of reversibly formed self-assembled cage complexes is far less common.[8] Performing reactions on self-assembled cage complexes is challenging,[9] and most known examples rely on very mild transformations, such as cycloadditions,[10] ring-closing metathesis,[11] CuAAc "click" reactions,[12] or the addition of species such as isocyanates.[13] These modifications are usually limited to the addition of new functional groups that do not disrupt the overall assembly.

In contrast, biological protein modifications change the overall macroscopic structure to provide new function to the molecule. Changing the structure and/or properties of self-assembled cage complexes via postassembly modification would add a wealth of new function to cage complexes.[14] The challenge is to identify suitably reactive cages that can be controllably modified, and the reaction conditions to do so. An ideal PAM would be CH oxidation[15] of methylene or methine groups in an unfunctionalized ligand backbone, as the initial cage synthesis is uncomplicated by the presence of reactive groups on the ligand. However, the postsynthetic reaction must be mild enough to maintain the discrete self-assembled structure and must occur without oxidation of the metal centers.[16] In addition, stereochemical control of the PAM is essential: there is no use in successfully oxidizing a cage complex only to introduce multiple stereoisomers of product. Here we show that hydrocarbon ligands in self-assembled cage complexes can be stereoselectively oxidized postassembly, without oxidation of the coordinating Fe(II) ions. The self-assembled structures direct and control the reaction outcomes, exploiting self-complementary hydrogen bonding or geometrical constraints to direct the postassembly reactions to outcomes not observed in free solution.

RESULTS AND DISCUSSION

To ensure that the oxidation could occur under mild conditions, we focused on doubly benzylic methylene units in the self-assembling ligand scaffolds, namely 2,7-diaminoxanthene **L1** and 2,7-diaminofluorene **L2** (Figure 1). Xanthene **L1** was synthesized in 3 steps from xanthone, via selective nitration followed by two separate reduction steps, to reduce the central carbonyl unit to an alcohol and then exhaustive reduction of the

Received: July 31, 2017

DOI: 10.1021/acs.inorgchem.7b01958
Inorg. Chem. XXXX, XXX, XXX–XXX

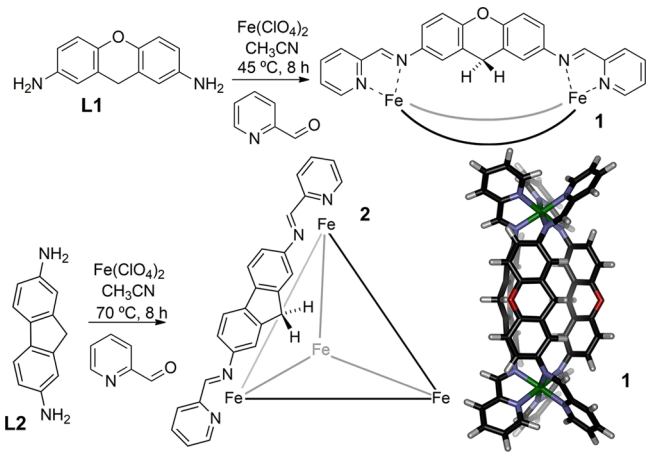

Figure 1. Multicomponent self-assembly of 2,7-diaminoxanthene **L1** into Fe_2L_3 *meso*-helicate **1** and of 2,7-diaminofluorene **L2** into Fe_4L_6 assembly **2**; molecular minimized structure of **1** (SPARTAN).

nitro groups and the alcohol to give **L1**. Diaminofluorene **L2** is easily accessed from reduction of commercially available dinitrofluorene. Xanthene ligand **L1** could be assembled into cage **1** via multicomponent self-assembly with $Fe(ClO_4)_2$ and 2-formylpyridine (PyCHO). The somewhat bent diaminoxanthene scaffold forms an Fe_2L_3 *meso*-helicate structure upon assembly, similar to that previously observed with 2,7-diaminoxanthone.[17] Electrospray ionization mass spectrometry (ESI-MS) analysis confirms this stoichiometry, and the mass spectrum mainly consists of variably charged perchlorate adducts of $Fe_2\mathbf{L1}_3$ (Figure 2f), namely the $Fe_2\mathbf{L1}_3\cdot(ClO_4)_3^+$, $Fe_2\mathbf{L1}_3\cdot(ClO_4)_2^{2+}$, and $Fe_2\mathbf{L1}_3\cdot ClO_4^{3+}$ ions. 1D and 2D NMR analysis (Figure 2a and Supporting Information) indicates a single diastereomer of the assembly is formed.

Treatment of **1** with ^{t}BuOOH (70% aqueous solution) in CH_3CN at 23 °C gave clean conversion to a new discrete complex (Figure 2). The reaction was complete after 5 h, and the product maintained the expected purple color throughout the reaction, indicating minimal Fe(II) oxidation had taken place. The ^{1}H NMR spectrum of the product **3** (Figure 2c) was sharp and discrete, with no evidence of paramagnetic Fe byproducts, but the spectrum of product **3** did not correspond to that of the expected tris-xanthone cage **4** (Figure 2d). CH oxidation of doubly benzylic methylene groups invariably forms the ketone as major product,[18] but not in the case of **1**. Diffusion NMR analysis of **3** shows that the product has a nearly identical diffusion constant to that of the xanthene cage **1** (D (**3**) = 1.859 × 10^{-9} m^2/s; D (**1**) = 1.794 × 10^{-9} m^2/s), suggesting that the product maintains the M_2L_3 *meso*-helicate stoichiometry. Further analysis via NMR and ESI-MS shows that the structure of product **3** is the *tris-tert*-butyl peroxide intermediate of the oxidation process. The mass spectrum is dominated by the $Fe_2L_3^{4+}$ fragment. A single, symmetric isomer of product is clearly formed, as can be seen by the ^{1}H NMR spectrum. The only symmetric isomer possibilities of **3** place the three OO^{t}Bu groups either *all-in* or *all-out*. Molecular modeling of **3** (see Figure 2 for a cross-section of the minimized structure) shows that the *all-out* isomer is the only realistic possibility, as significant steric clashes between inwardly facing OO^{t}Bu groups occur in the *all-in* conformation. 2D ROESY NMR corroborates the assignment of **3** as the *all-out* isomer, with NOE enhancements observed between the *tert*-butyl group and the distal backbone CH (*ortho* to the

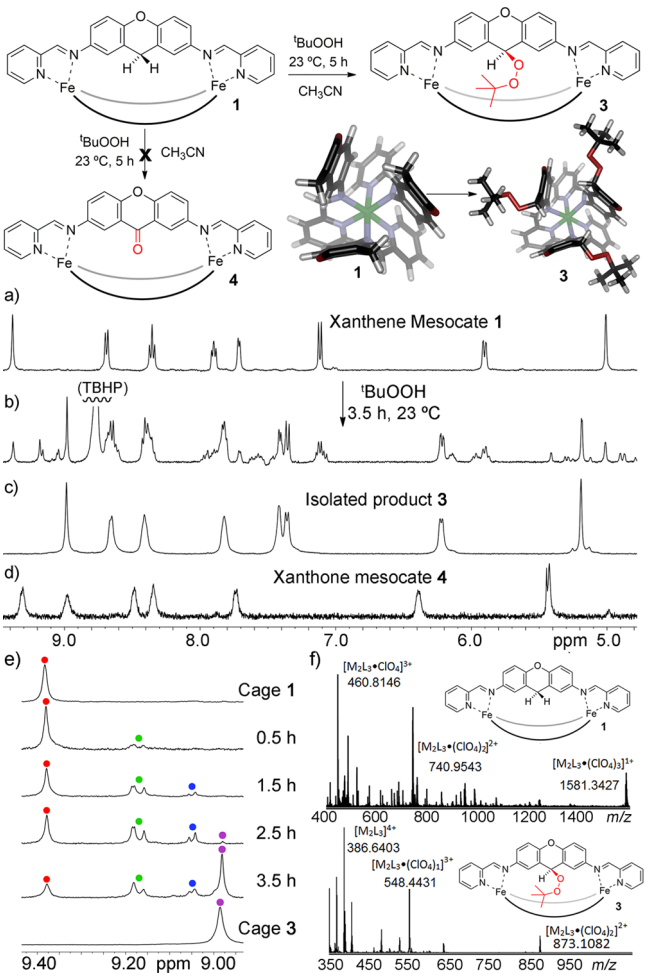

Figure 2. Ligand-centered oxidation of xanthene *meso*-helicate **1**: (a) ^{1}H NMR spectrum (600 MHz, CD_3CN, 298 K) of xanthene M_2L_3 *meso*-helicate **1**; (b) ^{1}H NMR spectrum of the reaction mixture of **1** and ^{t}BuOOH after 3.5 h at 23 °C; (c) ^{1}H NMR spectrum of the isolated product of reacting **1** with ^{t}BuOOH for 5 h at 23 °C; (d) ^{1}H NMR spectrum of independently prepared xanthone M_2L_3 *meso*-helicate **3**; (e) expanded ^{1}H NMR spectra (imine CH region) of the reaction of **1** and ^{t}BuOOH over time, illustrating reactant **1** (red), mono-oxidized (green), and dioxidized (blue) intermediates, and product **3** (purple); (f) ESI mass spectra of xanthene M_2L_3 *meso*-helicate **1** and the isolated product of reacting **1** with ^{t}BuOOH for 5 h at 23 °C.

xanthyl O, see Supporting Information for full assignment). The *tris-tert*-butylperoxide product **3** can be isolated by precipitation with ether, followed by washing, and is quite stable: no decomposition or conversion to other structures is observed upon heating at 70 °C for 3 days. Addition of a large excess of ^{t}BuOOH to the reaction did not cause any further oxidation, either of the ligand backbones or of the metal centers, even at 70 °C. The nature of the oxidant was important: oxone, mCPBA, and benzoyl peroxide gave no oxidation of **1**, and H_2O_2 or *N*-methylmorpholine *N*-oxide caused rapid decomposition.

The simple NMR spectrum of **1** allowed *in situ* reaction monitoring via ^{1}H NMR and clearly shows the mono- and dioxidized intermediates (Figure 2e), as reactant **1** is consumed and product **3** formed. Three peaks for each of the imine protons in the desymmetrized intermediates can be clearly seen, which collapse to a single symmetric peak in product **3**. At

DOI: 10.1021/acs.inorgchem.7b01958
Inorg. Chem. XXXX, XXX, XXX−XXX

no point during the reaction are any peaks observed for dissociated ligand or hydrolyzed diaminoxanthene **L1**, even in the presence of water from the ^{t}BuOOH solution. In addition, no other intermediates corresponding to ketone or hydroxyl oxidation products are seen: only sequential addition of *tert*-butyl peroxide functions to each ligand.

The simplicity and surprising outcome of the reaction of *meso*-helicate **1** with ^{t}BuOOH suggested the possibility that larger, more complex cages would be amenable to derivatization. We have previously shown that 2,7-diaminofluorenol forms the unusual M_4L_6 assembly **5** (Figure 3e) that favors a single diastereomeric conformation.[19] The observed *mer*$_3$*·fac* M_4L_6 prism structure is quite unusual,[20] templates one ClO_4^- ion, and H-bonding between the alcohols and the bound substrate directs the stereochemical outcome of the assembly. As diaminofluorene ligand **L2** displays a similar backbone to diaminofluorenol and has a similarly reactive methylene to **L1**, we envisioned that this would be a suitable component for self-assembled cage formation and oxidation. Upon treatment of **L2** with $Fe(ClO_4)_2$ and PyCHO, the characteristic purple color of a diamagnetic low spin Fe(II) iminopyridine assembly formed. The ^{1}H NMR spectrum of the Fe_4L_6 assembly **2** was unexpectedly complex, however (Figure 3a), even more so than the highly dissymmetric spectrum seen for **5**. Ligand **L2** has no prochiral centers, so cage **2** should display a more symmetric NMR spectrum than **5**.[21] Evidently, multiple metal-centered isomers of **2** are formed, and the assembly is uncontrolled. Many peaks in the ^{1}H NMR spectrum of **2** are similar to those of **5**, indicating that **2** partially exists as the *mer*$_3$*·fac* M_4L_6 prism structure (see Supporting Information for a partial assignment and full spectra data). While the complexity of the system precludes complete analysis of all the isomers present, it is reasonable to assume that the other isomers are *all-fac* tetrahedra with varying symmetry (T, S_4, and C_3), that are commonplace for cages of linear diamine precursors.[22] COSY and TOCSY analysis shows the presence of at least 8 dissymmetric methylenes in the system. ESI-MS analysis indicated the presence of only one stoichiometry of assembly with the majority of peaks in the spectrum corresponding to the series of ions $Fe_4L_6{\cdot}(ClO_4)_{1-5}^{3-7+}$, plus some other cage fragments. 2D DOSY analysis also indicates that all the isomers are consistent with Fe_4L_6 stoichiometry.

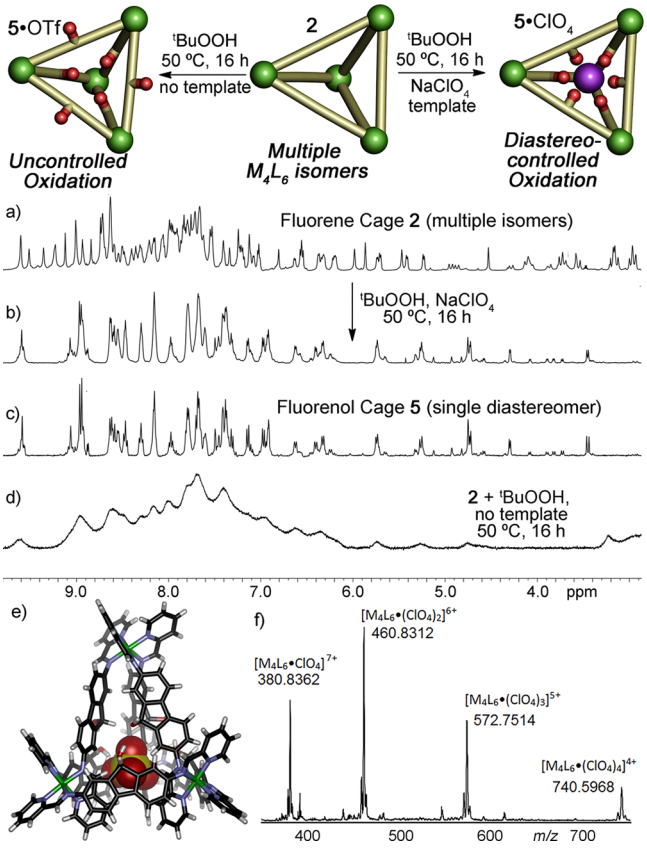

Figure 3. Ligand-centered oxidation of fluorene cage **2**. (a) ^{1}H NMR spectrum (600 MHz, CD_3CN, 298 K) of the multiple isomers of M_4L_6 fluorene cage **2**; (b) ^{1}H NMR spectrum of the product of reacting **2** with ^{t}BuOOH and $NaClO_4$; (c) ^{1}H NMR spectrum of independently prepared fluorenol cage **5**; (d) ^{1}H NMR spectrum of the product of reacting **2**·OTf with ^{t}BuOOH; (e) structure of **5** derived from X-ray diffraction analysis;[19] (f) ESI mass spectrum of the product of reacting **2** with ^{t}BuOOH and $NaClO_4$. L = dipyridylimine of 2,7-diaminofluorenol.

To shed light on how and why these reactions occur, we attempted a series of control experiments with xanthene and fluorene diamides **6** and **7** as surrogates for the nonassembled ligands. Xanthene control **6** was exposed to identical conditions required for complete conversion of **1** to **3**, i.e. 1.1 mol equiv of ^{t}BuOOH in CH_3CN at 23 °C for 5 h. Under these conditions, **6** is completely inert, and no conversion was observed even at 50 °C. When the reaction was performed in the presence of 10% $Fe(ClO_4)_2$, complete conversion of **6** was observed after 3.0 h at 23 °C. As expected, the product of oxidation of **6** was not the peroxide adduct, but xanthone **8**. Similarly, no reaction of fluorene **7** was observed in the absence of Fe(II), and fluorenone **9** was the major product observed upon addition of 10% $Fe(ClO_4)_2$, not the fluorenol equivalent.

The oxidation process requires Fe(II) catalyst: as there is only minimal free Fe(II) present in **1**/**2** after isolation and purification, two possibilities present themselves. Either small amounts of Fe(II) leach from the cages, allowing catalysis, or the cages themselves are catalytically active. The mechanism of Fe(II)-based hydrocarbon oxidation has been exhaustively studied, and Fe(II) catalysts require two free coordination sites to allow formation of the reactive Fe(V)-oxo species,[23] so it is unlikely that the intact cages are active catalysts. As can be seen in Table 1, when coordinatively saturated Fe-

DOI: 10.1021/acs.inorgchem.7b01958
Inorg. Chem. XXXX, XXX, XXX−XXX

Table 1. Outcomes of the Oxidation of Control Analogs.[a]

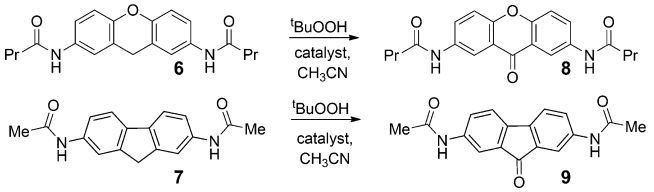

Substrate	*t*, h	*T*, °C	Catalyst	Product	Conversion, %
6	8	50	none	**8**	no rxn
6	1	23	10% $Fe(ClO_4)_2$	**8**	52
6	16	23	10% $Fe(Bipy)_3(ClO_4)_2$	**8**	4
6	1	23	10% cage **4**	**8**	58
7	8	50	none	**9**	no rxn
7	5	50	10% $Fe(ClO_4)_2$	**9**	45
7	16	50	10% $Fe(Bipy)_3(ClO_4)_2$	**9**	8
7	5	50	10% cage **4**	**9**	62

[a]1.1 mol equiv ^{t}BuOOH used.

$(bipy)_3(ClO_4)_2$ was used as catalyst, minimal reaction occurred. When 10% xanthone cage **4** was used, conversion was similar to that seen with free $Fe(ClO_4)_2$, giving products **8** and **9** in 58% and 62% conversion after 1 and 5 h, respectively. Evidently some leaching of Fe(II) salts occurs from the cages, which acts as a catalyst and is capable of oxidizing the remaining, intact cage. The observed yields of oxidation are from 88 to 93% for **1** (4 separate runs) and from 84 to 89% (3 separate runs) for the oxidation of **2**. It should be noted that no free ligand or disassembled cage was observed during the reaction of **1** (the complex NMR spectrum of **2** precludes accurate analysis). While some Fe(II) is lost from the starting cage during the reaction, it can only be a small percentage of the material, and the reactions are remarkably efficient. In addition, the coordinating Fe(II) ions of the product assembly are unaffected: oxidation occurs selectively on the ligand backbone, despite some Fe(II) ions leaching from the assembly.

The fact that the ligand-centered oxidations of both **1** and **2** occur at all is remarkable, considering their reversible assembly and general fragility toward nucleophiles. In addition, the reaction outcomes are altered, and directed by the self-assembled structure. Given the option, free Fe(II) salts oxidize fluorenyl and xanthenyl substrates to ketones with ^{t}BuOOH. The mechanism is well-known[24] and occurs via formation of a reactive Fe═O species that abstracts a hydrogen atom from the CH_2, leaving a stabilized radical that can recombine with either $^{\bullet}$OH, $^{\bullet}$O^{t}Bu, or $^{\bullet}$OO^{t}Bu radicals, all created by the reaction of ^{t}BuOOH with Fe(II) salts (Figure 4).[25] These alcohol or peroxide adducts are more reactive than the parent hydrocarbon, and so a second oxidation occurs to form the ketone. The answer to why the expected ketone products are not formed from oxidation of **1** and **2** lies in the stability of the products formed, or more precisely the *unfavorability* of the ketone cages (Figure 4a). Diaminoxanthone cage **4** provides a poor coordination geometry for M_2L_3 complex formation, and the strained *meso*-helicate **4** is relatively unstable.[17] While the vast majority of Fe-iminopyridine assemblies are diamagnetic low spin Fe(II) complexes, **4** shows a deep red color and temperature-dependent ^{1}H NMR shifts, indicating paramagnetism and intermediate spin Fe(II) centers.[26] Xanthene *meso*-helicate **1** is diamagnetic and far more stable, as can be illustrated by competition experiments. When **L1** is added to freshly made **4** in CD_3CN, complete displacement of

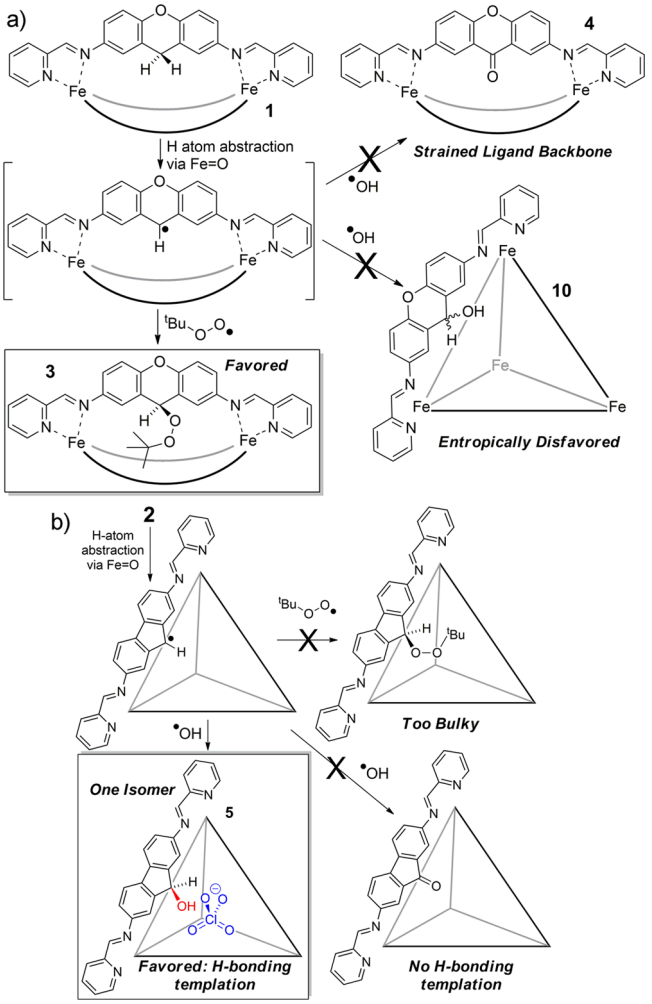

Figure 4. Outcomes of ligand-centered CH oxidation. (a) Xanthene M_2L_3 *meso*-helicate forms the peroxide adduct **3** to avoid the highly strained ketone **4** or the entropically disfavored M_4L_6 alcohol **10**; (b) Uncontrolled fluorene M_4L_6 assembly **2** exploits favorable H-bonding to form a single isomer of alcohol prism **5**.

diaminoxanthone occurs after 4 h at 45 °C (see Supporting Information). In contrast, xanthene *meso*-helicate **1** is completely impervious to displacement by 2,7-diaminoxan-

DOI: 10.1021/acs.inorgchem.7b01958
Inorg. Chem. XXXX, XXX, XXX−XXX

thone, even after 24 h at 70 °C. The peroxide *meso*-helicate oxidation product **3** is also more stable than xanthone *meso*-helicate **4**. No displacement of peroxide ligand from *meso*-helicate **3** was observed after heating with 2,7-diaminoxanthone at 70 °C for 24 h. Interestingly, xanthene **1** is more stable than peroxide **3**: diaminoxanthene **L1** was able to cleanly displace the oxidation product ligand after 8 h at 70 °C.

The ketone cage is unstable and disfavored, but the other obvious outcome of oxidation of **1** would be to form the hydroxylated product. To establish why this species is not formed, we studied the assembly of 2,7-diaminoxanthol with $Fe(ClO_4)_2$ and PyCHO. Most surprisingly, 2,7-diaminoxanthol did not form an M_2L_3 *meso*-helicate upon assembly as expected but forms cage product **10**, with Fe_4L_6 stoichiometry. The assembly is stereochemically uncontrolled, as illustrated by the highly complex ^{1}H NMR spectrum (see Supporting Information). ESI-MS analysis cleanly shows the presence of $Fe_4L_6{\cdot}(ClO_4)_x^{y+}$ ion clusters: only peaks for $Fe_4L_6{\cdot}(ClO_4)_5^{3+}$, $Fe_4L_6{\cdot}(ClO_4)_4^{4+}$, $Fe_4L_6{\cdot}(ClO_4)_3^{6+}$, and $Fe_4L_6^{8+}$ were present. Interestingly, the parent $Fe_4L_6{\cdot}(ClO_4)_x^{y+}$ ion clusters were accompanied by ions corresponding to additional loss of water from the assembly, presumably at the xanthol OH center. The complex also loses water upon standing in the solid state, and elemental analysis indicates that between 2 and 3 water molecules are lost from the cage in under 24 h. While the ^{1}H NMR spectrum is far too complex to be assigned, 2D DOSY analysis shows that all peaks have identical diffusion constants (D (**10**) = 8.497×10^{-10} m^2/s), similar to those of cage **5** (D = 9.883×10^{-10} m^2/s), but much smaller than that of the M_2L_3 *meso*-helicate **1** (D = 1.794×10^{-9} m^2/s). It is not clear why 2,7-diaminoxanthol assembles into an unstable, uncontrolled M_4L_6 system when all other xanthyl ligands tested form M_2L_3 helicates, but the self-assembly process is obviously disfavored. Formation of the M_4L_6 assembly upon oxidation of **1** would require reorganization of the assembly into a larger, entropically disfavored assembly, and so the oxidation reaction stops at the more favorable *tris*-peroxide intermediate **3**. Notably, 2,7-diaminoxanthol is unable to displace the peroxide ligand from **3**, even when heated to 70 °C overnight.

The formation of fluorenol cage **5** upon oxidation of **2** is also directed by the stability of the product (Figure 4b). Both diaminofluorene and diaminofluorenone form complex isomeric mixtures of M_4L_6 cages upon multicomponent self-assembly, whereas the ClO_4^- templated fluorenol cage **5** is favored by intracage H-bonds. This H-bonding is sufficient to direct the reaction, and as such **5**·ClO_4 is the only observed reaction product. When the oxidation reaction is performed on **2**·OTf, multiple uncontrolled products are formed. Only when $NaClO_4$ is added to the oxidation reaction does a single product form, indicating that the fluorene cage oxidation process is thermodynamically controlled. The templated fluorenol cage is the only favored product and occurs via equilibration under the reaction conditions in the presence of a suitable templating ion.

In addition to directing the product outcome, the cage structures direct the stereochemical outcomes: oxidation of xanthene *meso*-helicate **1** gives the *all-out* diastereomer of **3**, and oxidation of fluorene cage **2** yields a single diastereomer of Fe_4L_6 prism **5**. In each case the stability of the product and the reversibility of the assembly control the stereochemical outcome. It is certainly conceivable that oxidation of **1** occurs only on the exterior face of the *meso*-helicate, as the M_2L_3 assembly remains mainly intact throughout the reaction, other than the small amount of dissociation required to give sufficient free Fe(II) for catalysis. Ligand exchange in Fe_2L_3 helicates occurs rapidly, however, and so equilibration of the product to the most favorable isomer can easily occur under these reaction conditions. It is likely that the kinetic and thermodynamic product is the same in this case: there is no internal cavity, and all other isomers are repulsively disfavored. While the product outcome of the oxidation of **2** is different from that of **1**, the self-assembled structure also directs the reaction stereochemistry: in this case, favorable H-bonding directs the oxidation away from the expected ketone to the hexa-hydroxyl product. The stereochemical fidelity is even more impressive: whereas **3** has no cavity, and the *all-out* isomer is obviously most stable due to steric effects, only self-complementary H-bonding directs the formation of **5**·$(ClO_4)_8$.

CONCLUSIONS

Here, we have shown that postassembly modification of reversibly formed, self-assembled cage complexes can be controlled and directed by the self-assembled structure. Ligand centered CH oxidation reactions can occur on Fe(II)-containing self-assembled cages, and exploit small amounts of Fe(II) ions as catalysts for the transformations, leached from the assemblies. Despite this, excellent yields of diastereocontrolled oxidation products can be obtained with no oxidation of the coordinating Fe(II) centers. The structure of the assemblies controls the reaction outcome: while nonassembled ligands favor oxidation to the ketone, the oxidation of the xanthene and fluorene cages forms the ^{t}butyl peroxide and alcohol-containing oxidation cage products, respectively. The introduction of stereocenters to the products allows the reactions to be stereocontrolled, and excellent diastereoselectivity is seen, with only single isomers formed despite the presence of multiple new stereocenters in the final product. The self-assembled structures exploit either self-complementary hydrogen bonding or geometrical constraints to direct the postassembly reactions to outcomes not observed in free solution. Further work on applying this exquisite structural control to functional assemblies is underway.

EXPERIMENTAL SECTION

General. ^{1}H and ^{13}C NMR spectra were recorded on a Varian Inova 400, Varian Inova 500, or Bruker Avance 600 MHz NMR spectrometer. Proton (^{1}H) and carbon (^{13}C) chemical shifts are reported in parts per million (δ) with respect to tetramethylsilane (TMS, δ = 0), and referenced internally with respect to the protio solvent impurity or residual ^{13}C solvent signal. Deuterated NMR solvents were obtained from Cambridge Isotope Laboratories, Inc., Andover, MA, and used without further purification. Mass spectrometric analysis was performed using a Thermo LTQ linear ion trap with a standard electrospray ionization source (Thermo Fisher Scientific, San Jose, CA, USA). Samples were directly infused at 3 μL/min in 100% MeCN, with the source voltage set to 3 kV, tube lens at 75 kV, and the capillary temperature at 270 °C. CID spectra were collected in ZoomScan mode where the isolation window = 5 m/z, normalized collision energy (nCE) = 30, and activation time = 30 ms. MS data was analyzed using Thermo XCalibur. Predicted isotope patterns were prepared using ChemCalc. All other materials were obtained from Aldrich Chemical Co. (St. Louis, MO), or Fisher Scientific (Fairlawn, NJ), and were used as received. Solvents were dried through a commercial solvent purification system (Pure Process Technologies, Inc.). Xanthone *meso*-helicate **4**[17] and fluorenol prism **5**[19] were synthesized according to literature procedures.

Synthesis of Compounds. *2,7-Dinitroxanthol.* 2,7-Dinitroxanthone (1.00 g, 3.49 mmol) was placed in a 250 mL round bottomed

DOI: 10.1021/acs.inorgchem.7b01958
Inorg. Chem. XXXX, XXX, XXX−XXX

flask and dissolved in 100 mL of dry tetrahydrofuran and 25 mL of methanol. Sodium borohydride (150 mg, 3.97 mmol) was slowly added to the flask, and the reaction was allowed to stir at room temperature. After 12 h, a second portion of sodium borohydride (30 mg) was added to the flask and the reaction stirred for 1 h. The reaction mixture was then poured into a beaker containing 500 mL of ice water. The mixture was rapidly stirred and brought to a pH of 3 using 1 M hydrochloric acid. The product was then filtered and collected as a tan solid (942 mg, 94%). ^{1}H NMR (400 MHz, DMSO-d_6): δ 8.46 (d, J = 2.7 Hz, 2H), 8.23 (dd, J = 9.0, 2.7 Hz, 2H), 7.46 (d, J = 9.1 Hz, 2H), 6.84 (d, J = 6.8 Hz, 1H), 5.90 (d, J = 6.5 Hz, 1H). ^{13}C NMR (100 MHz, DMSO-d_6): δ 154.2, 144.2, 126.1, 125.4, 124.7, 118.5, 60.7. HRMS (ESI) m/z calcd. for $C_{13}H_9N_2O_6$ ([M·H]$^+$) 289.0234, found 289.0259.

*2,7-Diaminoxanthene (Dianiline **L1**).* 2,7-Dinitroxanthol (300 mg, 1.1 mmol) was placed in a long-necked Schlenk flask with a septum and stir bar and the flask was purged with nitrogen. Methanol (15 mL) and a large excess of Raney nickel slurry in water (5 mL) were injected into the flask, and the system was quickly purged with nitrogen a second time. Hydrazine monohydrate (1 mL) was slowly injected into the flask and the reaction allowed to stir overnight at room temperature. The mixture was diluted with additional methanol (25 mL) and the solid catalyst was carefully removed via filtration through a Celite plug. The filtrate solvent was removed *in vacuo* to afford clean product as a pale yellow solid (291 mg, 94%). ^{1}H NMR (400 MHz, DMSO-d_6): δ 6.65 (d, J = 8.1 Hz, 2H), 6.37 (m, 4H), 4.67 (s, 4H), 3.71 (s, 2H). ^{13}C NMR (100 MHz, DMSO-d_6): δ 144.4, 143.8, 121.0, 116.7, 114.2, 113.9, 28.4. HRMS (ESI) m/z calcd. for $C_{13}H_{13}N_2O$ ([dianiline **L1**·H]$^+$) 213.0493, found 213.1062.

*Xanthene Cage **1**.* Dianiline **L1** (100 mg, 0.47 mmol), 2-pyridine carboxaldehyde (90 μL, 0.94 mmol), and $Fe(ClO_4)_2{\cdot}H_2O$ (103 mg, 0.31 mmol) were combined in anhydrous acetonitrile (10 mL) in a 25 mL round-bottomed flask under a blanket of nitrogen gas. The solution was heated at 45 °C for 10 h with stirring. The reaction was diluted with diethyl ether (25 mL), and the resulting precipitate was filtered. After drying, the product was isolated as a purple solid (201 mg, 93%). ^{1}H NMR (400 MHz; CD_3CN) δ 9.38 (s, 2H), 8.69 (d, J = 7.5 Hz, 2H), 8.35 (t, J = 7.3 Hz, 2H), 7.9 (t, J = 5.4 Hz, 2H), 7.71 (d, J = 5.1 Hz, 2H), 7.12 (d, J = 8.1 Hz, 2H), 5.9 (d, J = 6.9 Hz, 2H), 5.01 (s, 2H), 3.55 (d, J = 19.9 Hz, 1H) 2.72 (d, J = 19.9 Hz, 1H). ^{13}C NMR (125 MHz, CD_3CN): δ 173.6, 157.1, 156.1, 151.4, 148.2, 139.6, 132.2, 131.4, 124.1, 121.7, 121.0, 27.5. HRMS (ESI) m/z calcd. for $C_{75}H_{54}Cl_3Fe_2N_{12}O_{15}$ ([**1**•$(ClO_4)_3$]$^+$) 1581.3561, found 1581.3427. Elemental Analysis: Calc. for $C_{75}H_{54}Cl_4Fe_2N_{12}O_{19}$ C: 53.59; H: 3.24; N: 10.01; Found: C: 53.46; H: 3.35; N: 9.97.

*Oxidation of meso-Helicate **1** to Xanthyl Peroxide Cage **3**.* One equivalent of xanthene *meso*-helicate **1** (30 mg, 0.018 mmol) was dissolved in 2 mL of acetonitrile in a 10 mL round bottomed flask. 3.3 mol equiv of *tert*-butyl hydroperoxide 70% solution in water (7.6 μL 0.059 mmol) was then added, and the reaction mixture was allowed to stir at room temperature for 8 h. Diethyl ether (10 mL) was then added to the solution, and xanthyl peroxide cage **3** precipitated as a purple solid that was filtered and dried (29 mg, 88%). ^{1}H NMR (400 MHz; CD_3CN) δ 8.99 (s, 2H), 8.65 (d, J = 7.4 Hz, 2H), 8.41 (t, J = 7.5 Hz, 2H), 7.82 (t, J = 7.4 Hz, 2H), 7.41 (d, J = 5.3 Hz, 2H), 7.36 (d, J = 8.7 Hz, 2H), 6.22 (dd, J = 8.6, 2.6 Hz, 2H), 5.19 (s, 2H), 4.11 (s, 1H), 1.14 (s, 9H).^{13}C NMR (125 MHz, CD_3CN) δ 175.4, 157.5, 156.1, 151.7, 147.4, 139.7, 132.1, 130.5, 124.7, 124.5, 119.1, 117.8, 80.7, 72.9, 25.6. HRMS (ESI) m/z calcd. for $C_{87}H_{78}Fe_2N_{12}O_9$ (**3**$^{4+}$) 386.5788, found 386.6403. Elemental Analysis: Calc. for $C_{87}H_{78}Cl_4Fe_2N_{12}O_{25}$ C: 53.72; H: 4.04; N: 8.64; Found: C: 53.67; H: 4.10; N: 8.58.

*Fluorene Cage **2**.* 2,7-Diaminofluorene **L2** (100 mg, 0.51 mmol), 2-pyridine carboxaldehyde (96.9 μL, 1.02 mmol), and $Fe(ClO_4)_2{\cdot}4H_2O$ (111 mg, 0.34 mmol) were combined in anhydrous acetonitrile (10 mL) in a 50 mL Schlenk flask under a nitrogen atmosphere, followed by heating to 60 °C for 10 h. The solution was cooled to room temperature and diluted with diethyl ether (30 mL), and the resulting precipitate was filtered. Product was collected as a purple solid (187 mg, 94%). ^{1}H NMR and ^{13}C NMR: Complex mixture of isomers. See SI Figures **S28** through **S40** for relevant NMR and ESI spectra. HRMS (ESI) m/z calcd for $C_{150}H_{108}Cl_8Fe_4N_{24}O_{32}$ ([**2**·$(ClO_4)_2$]$^{6+}$) 444.5932, found 444.8816. Elemental Analysis: Calc. for $C_{150}H_{108}Cl_8Fe_4N_{24}O_{32}$ C: 55.17; H: 3.33; N: 10.29; Found: C: 55.25; H: 3.37; N: 10.39.

*Oxidation of Fluorene Cage **2** to Fluorenol Cage **5**.* One equivalent of fluorene cage **2** (30 mg, 0.009 mmol) was dissolved in acetonitrile (2 mL) in a 10 mL round bottomed flask. *tert*-Butyl hydroperoxide 70% solution in water (7.6 μL, 0.055 mmol) and sodium perchlorate (1 mg) were added, and the reaction was allowed to stir at 50 °C for 24 h. Diethyl ether (10 mL) was added to the solution, and fluorenol cage **5** precipitated as a purple solid that was filtered and dried (28 mg, 87%). ^{1}H NMR and ^{13}C NMR were consistent with published spectra.[19] See SI Figures **S41** through **S44** for relevant NMR and ESI spectra. HRMS (ESI) m/z calcd for $C_{150}H_{108}Cl_2Fe_4N_{24}O_{14}$ ([**5**·$(ClO_4)_2$]$^{6+}$) 460.5881, found 460.8312.

*2,7-Diaminoxanthol (Dianiline **L3**).* 2,7-Dinitroxanthol (600 mg, 2.1 mmol) was placed in a Schlenk flask with a septum and stir bar, and the flask was purged several times with nitrogen. Methanol (10 mL) and Raney nickel slurry in water (0.2 mL) were injected into the flask, and the system was quickly purged with nitrogen a second time. Hydrazine monohydrate (0.4 mL) was slowly injected into the flask. The mixture was allowed to stir for 6 h at room temperature. The solid catalyst was carefully filtered off over a firmly packed Celite plug. Dichloromethane (20 mL) was added to the filtrate, and the solution was washed with brine (2 × 15 mL). The organic layer was dried with $MgSO_4$ and the solvent removed *in vacuo* to afford crude product as an orange solid (393 mg, 82%). The product was purified via selective Boc-protection of the amines, followed by column chromatography (5% ethyl acetate in hexanes), and BOC-deprotection with hydrochloric acid in diethyl ether followed by neutralization.[17] ^{1}H NMR (400 MHz, DMSO-d_6): δ 6.73 (d, J = 8.6 Hz, 2H), 6.68 (d, J = 1.8 Hz, 2H), 6.49 (dd, J = 8.6, 2.7 Hz, 1H), 5.60 (d, J = 7.7 Hz, 1H), 5.33 (d, J = 7.7 Hz, 1H), 4.73 (s, 4H). ^{13}C NMR (125 MHz, CD_3CN): δ 143.5, 143.2, 123.7, 116.5, 116.2, 114.1, 63.2. HRMS (ESI) m/z calcd. for $C_{13}H_{13}N_2O_2$ ([dianiline **L3**·H]$^+$) 229.0493, found 229.1062.

*Xanthol Cage **10**.* Dianiline **L3** (25 mg, 0.11 mmol), 2-pyridine carboxaldehyde (21 μL, 0.22 mmol), and $Fe(ClO_4)_2{\cdot}4H_2O$ (24 mg, 0.08 mmol) were combined in anhydrous acetonitrile (5 mL) in a 10 mL round-bottomed flask under a blanket of nitrogen, followed by heating to 45 °C for 10 h. The solution was then cooled to room temperature and diluted with diethyl ether (30 mL), and the resulting precipitate was filtered. Drying the solid *in vacuo* gave product as a purple solid (49 mg, 98%). ^{1}H NMR and ^{13}C NMR: Complex mixture of stereoisomers. See SI figures **S52** through **S55** for relevant NMR and ESI spectra. HRMS (ESI) m/z calcd for $C_{150}H_{108}Cl_5Fe_4N_{24}O_{32}$ ([**10**·$(ClO_4)_5$]$^{3+}$) 1053.0846, found 1053.0830. Elemental Analysis: Calc. for $C_{150}H_{105}Cl_8Fe_4N_{24}O_{41}$ (loss of 3 x H_2O) C: 52.89; H: 3.11; N: 9.87 and $C_{150}H_{106}Cl_8Fe_4N_{24}O_{42}$ (loss of 2 ×x H_2O) C: 52.62; H: 3.12; N: 9.81; Found: C: 52.73; H: 3.13; N: 9.85.

General Procedure for Control Ligand Oxidations. Xanthene control ligand **6** (25 mg, 0.072 mmol) was placed in in a 10 mL round bottomed flask and dissolved in acetonitrile (5 mL). *tert*-Butyl hydroperoxide 70% solution in water (10.1 μL 0.078 mmol) and catalytic $Fe(ClO_4)_2{\cdot}4H_2O$ (0.2 mg, 0.007 mmol) were added. The reaction was allowed to stir at room temperature (or at 50 °C) for 8 h. Chloroform (5 mL) was added to the flask, and the reaction products were extracted with brine (2 × 5 mL). The organic layer was dried with $MgSO_4$, and the solvent was removed *in vacuo*. All products were obtained in 89−95% yields; see SI for full characterization and details. The spectra of the oxidation products was compared to those of independently synthesized ketone and alcohol products.

■ ASSOCIATED CONTENT

Supporting Information

The Supporting Information is available free of charge on the ACS Publications website at DOI: 10.1021/acs.inorgchem.7b01958.

Characterization and synthetic procedures not described in the text and spectral data (PDF)

DOI: 10.1021/acs.inorgchem.7b01958
Inorg. Chem. XXXX, XXX, XXX−XXX

AUTHOR INFORMATION

Corresponding Author

*E-mail: richard.hooley@ucr.edu.

ORCID

Ryan R. Julian: 0000-0003-1580-8355

Richard J. Hooley: 0000-0003-0033-8653

Notes

The authors declare no competing financial interest.

ACKNOWLEDGMENTS

This work is sponsored by the National Science Foundation (CHE-1151773 to R.J.H. and CHE-1401737 to R.R.J). The authors would like to thank Dr. Dan Borchardt for NMR assistance.

REFERENCES

(1) Sonenberg, N.; Hinnebusch, A. G. Regulation of translation initiation in eukaryotes: mechanisms and biological targets. *Cell* **2009**, *136*, 731−745.

(2) Bah, A.; Vernon, R. M.; Siddiqui, Z.; Krzeminski, M.; Muhandiram, R.; Zhao, C.; Sonenberg, N.; Kay, L. E.; Forman-Kay, J. D. Folding of an intrinsically disordered protein by phosphorylation as a regulatory switch. *Nature* **2015**, *519*, 106−109.

(3) (a) Murase, T.; Horiuchi, S.; Fujita, M. Naphthalene Diels−alder in a self-assembled molecular flask. *J. Am. Chem. Soc.* **2010**, *132*, 2866−2867. (b) Fiedler, D.; van Halbeek, H.; Bergman, R. G.; Raymond, K. N. Supramolecular catalysis of unimolecular rearrangements: substrate scope and mechanistic insights. *J. Am. Chem. Soc.* **2006**, *128*, 10240−10252. (c) Leung, D. H.; Fiedler, D.; Bergman, R. G.; Raymond, K. N. Selective C-H bond activation by a supramolecular host-guest assembly. *Angew. Chem., Int. Ed.* **2004**, *43*, 963−966.

(4) (a) Kaphan, D. M.; Levin, M. D.; Bergman, R. G.; Raymond, K. N.; Toste, F. D. A supramolecular microenvironment strategy for transition metal catalysis. *Science* **2015**, *350*, 1235−1238. (b) Hastings, C. J.; Pluth, M. D.; Bergman, R. D.; Raymond, K. N. Enzymelike catalysis of the Nazarov cyclization by supramolecular encapsulation. *J. Am. Chem. Soc.* **2010**, *132*, 6938−6940. (c) Cullen, W.; Misuraca, M. C.; Hunter, C. A.; Williams, N. H.; Ward, M. D. Highly efficient catalysis of the Kemp elimination in the cavity of a cubic coordination cage. *Nat. Chem.* **2016**, *8*, 231−236. (d) Wang, Q.-Q.; Gonell, S.; Leenders, S. H. A. M.; Dürr, M.; Ivanović-Burmazović, I.; Reek, J. N. H. Self-assembled nanospheres with multiple endohedral binding sites pre-organize catalysts and substrates for highly efficient reactions. *Nat. Chem.* **2016**, *8*, 225−230. (e) Levin, M. D.; Kaphan, D. M.; Hong, C. M.; Bergman, R. G.; Raymond, K. N.; Toste, F. D. Scope and mechanism of cooperativity at the intersection of organometallic and supramolecular catalysis. *J. Am. Chem. Soc.* **2016**, *138*, 9682−9693. (f) Qiao, Y.; Zhang, L.; Li, J.; Lin, W.; Wang, Z. Switching on supramolecular catalysis via cavity mediation and electrostatic regulation. *Angew. Chem., Int. Ed.* **2016**, *55*, 12778−12782. (g) Brown, C. J.; Toste, F. D.; Bergman, R. G.; Raymond, K. N. Supramolecular catalysis in metal-ligand cluster hosts. *Chem. Rev.* **2015**, *115*, 3012−3035.

(5) (a) Mal, P.; Breiner, B.; Rissanen, K.; Nitschke, J. R. White phosphorus is air-stable within a self-assembled tetrahedral capsule. *Science* **2009**, *324*, 1697−1699. (b) Horiuchi, S.; Murase, T.; Fujita, M. A remarkable organometallic transformation on a cage-incarcerated dinuclear ruthenium complex. *Angew. Chem., Int. Ed.* **2012**, *51*, 12029−12031. (c) Ward, M. D.; Raithby, P. R. Functional behaviour from controlled self-assembly: challenges and prospects. *Chem. Soc. Rev.* **2013**, *42*, 1619−1636.

(6) (a) Yoshizawa, M.; Tamura, M.; Fujita, M. Diels-alder in aqueous molecular hosts: unusual regioselectivity and efficient catalysis. *Science* **2006**, *312*, 251−254. (b) Zhao, C.; Toste, F. D.; Bergman, R. G.; Raymond, K. N. Nucleophilic substitution catalyzed by a supramolecular cavity proceeds with retention of absolute stereochemistry. *J. Am. Chem. Soc.* **2014**, *136*, 14409−14412.

(7) Tanabe, K. K.; Cohen, S. M. Postsynthetic modification of metal-organic frameworks-a progress report. *Chem. Soc. Rev.* **2011**, *40*, 498−519.

(8) (a) Acharyya, K.; Mukherjee, P. S. Postsynthetic exterior decoration of an organic cage by copper(I)-catalysed A^3-coupling and detection of nitroaromatics. *Chem. - Eur. J.* **2015**, *21*, 6823−6831. (b) Sun, Q.-F.; Sato, S.; Fujita, M. An $M_{18}L_{24}$ stellated cuboctahedron through post-stellation of an $M_{12}L_{24}$ core. *Nat. Chem.* **2012**, *4*, 330−333. (c) Zheng, Y.-R.; Lan, W.-J.; Wang, M.; Cook, T. R.; Stang, P. J. Designed post-self-assembly structural and functional modifications of a truncated tetrahedron. *J. Am. Chem. Soc.* **2011**, *133*, 17045−17055. (d) Glasson, C. R. K.; Meehan, G. V.; Davies, M.; Motti, C. A.; Clegg, J. K.; Lindoy, L. F. Post-assembly covalent di- and tetracapping of a dinuclear $[Fe_2L_3]^{4+}$ triple helicate and two $[Fe_4L_6]^{8+}$ tetrahedra using sequential reductive aminations. *Inorg. Chem.* **2015**, *54*, 6986−6992.

(9) (a) Wang, M.; Lan, W.-J.; Zheng, Y.-R.; Cook, T. R.; White, H. S.; Stang, P. J. Post-self-assembly covalent chemistry of discrete multicomponent metallosupramolecular hexagonal prisms. *J. Am. Chem. Soc.* **2011**, *133*, 10752−10755. (b) Samanta, D.; Chowdhury, A.; Mukherjee, P. S. Covalent postassembly modification and water adsorption of Pd_3 self-assembled trinuclear barrels. *Inorg. Chem.* **2016**, *55*, 1562−1568.

(10) (a) Roberts, D. A.; Pilgrim, B. S.; Cooper, J. D.; Ronson, T. K.; Zarra, S.; Nitschke, J. R. Post-assembly modification of tetrazine-edged $Fe^{II}_4L_6$ tetrahedra. *J. Am. Chem. Soc.* **2015**, *137*, 10068−10071. (b) Ronson, T. K.; Pilgrim, B. S.; Nitschke, J. R. Pathway-dependent post-assembly modification of an anthracene-edged $M^{II}_4L_6$ tetrahedron. *J. Am. Chem. Soc.* **2016**, *138*, 10417−10420. (c) Barran, P. E.; Cole, H. L.; Goldup, S. M.; Leigh, D. A.; McGonigal, P. R.; Symes, M. D.; Wu, J.; Zengerle, M. Active-metal template synthesis of a molecular trefoil knot. *Angew. Chem., Int. Ed.* **2011**, *50*, 12280−12284.

(11) (a) Hiraoka, S.; Yamauchi, Y.; Arakane, R.; Shionoya, M. Template-directed synthesis of a covalent organic capsule based on a 3 nm-sized metallocapsule. *J. Am. Chem. Soc.* **2009**, *131*, 11646−11647. (b) Leigh, D. A.; Pritchard, R. G.; Stephens, A. J. A Star of David catenane. *Nat. Chem.* **2014**, *6*, 978−982. (c) Fuller, A.-M. L.; Leigh, D. A.; Lusby, P. J.; Slawin, A. M. Z.; Walker, D. B. Selecting topology and connectivity through metal-directed macrocyclization reactions:a square planar palladium [2]catenate and two noninterlocked isomers. *J. Am. Chem. Soc.* **2005**, *127*, 12612−12619. (d) Leigh, D. A.; Lusby, P. J.; McBurney, R. T.; Morelli, A.; Slawin, A. M. Z.; Thomson, A. R.; Walker, D. B. Getting harder: cobalt(III)-template synthesis of catenanes and rotaxanes. *J. Am. Chem. Soc.* **2009**, *131*, 3762−3771.

(12) Chakrabarty, R.; Stang, P. J. Post-assembly functionalization of organoplatinum(II) metallacycles via copper-free click chemistry. *J. Am. Chem. Soc.* **2012**, *134*, 14738−14741.

(13) (a) Roberts, D. A.; Castilla, A. M.; Ronson, T. K.; Nitschke, J. R. Post-assembly modification of kinetically metastable $Fe^{II}_2L_3$ triple helicates. *J. Am. Chem. Soc.* **2014**, *136*, 8201−8204. (b) Young, M. C.; Johnson, A. M.; Hooley, R. J. Self-promoted post-synthetic modification of metal-ligand M_2L_3 mesocates. *Chem. Commun.* **2014**, *50*, 1378−1380. (c) Brega, V.; Zeller, M.; He, Y.; Lu, P. H.; Klosterman, J. K. Multi-responsive metal−organic lantern cages in solution. *Chem. Commun.* **2015**, *51*, 5077−5080.

(14) (a) Han, M.; Michel, R.; He, B.; Chen, Y.-S.; Stalke, D.; John, M.; Clever, G. H. Light-triggered guest uptake and release by a photochromic coordination cage. *Angew. Chem., Int. Ed.* **2013**, *52*, 1319−1323. (b) Castilla, A. M.; Ronson, T. K.; Nitschke, J. R. Sequence-dependent guest release triggered by orthogonal chemical signals. *J. Am. Chem. Soc.* **2016**, *138*, 2342−2351.

(15) (a) Newhouse, T.; Baran, B. S. If C−H bonds could talk − selective C−H bond oxidation. *Angew. Chem., Int. Ed.* **2011**, *50*, 3362−3374. (b) Chen, M. S.; White, M. C. A predictably selective aliphatic C-H oxidation reaction for complex molecule synthesis. *Science* **2007**, *318*, 783−787.

(16) (a) Burke, M. J.; Nichol, G. S.; Lusby, P. J. Orthogonal selection and fixing of coordination self-assembly pathways for robust metallo-

DOI: 10.1021/acs.inorgchem.7b01958
Inorg. Chem. XXXX, XXX, XXX−XXX

organic ensemble construction. *J. Am. Chem. Soc.* **2016**, *138*, 9308−9315. (b) Symmers, P. R.; Burke, M. J.; August, D. P.; Thomson, P. I. T.; Nichol, G. S.; Warren, M. R.; Campbell, C. J.; Lusby, P. J. Non-equilibrium cobalt(III) "click" capsules. *Chem. Sci.* **2015**, *6*, 756−760.
(17) Holloway, L. R.; Young, M. C.; Beran, G. J. O.; Hooley, R. J. High fidelity sorting of remarkably similar components via metal-mediated assembly. *Chem. Sci.* **2015**, *6*, 4801−4806.
(18) Chen, M. S.; White, M. C. Combined effects on selectivity in Fe-catalyzed methylene oxidation. *Science* **2010**, *327*, 566−571.
(19) Young, M. C.; Holloway, L. R.; Johnson, A. M.; Hooley, R. J. A supramolecular sorting hat: stereocontrol in metal−ligand self-assembly by complementary hydrogen bonding. *Angew. Chem., Int. Ed.* **2014**, *53*, 9832−9836.
(20) (a) Riddell, I. A.; Smulders, M. M. J.; Clegg, J. K.; Hristova, Y. R.; Breiner, B.; Thoburn, J. D.; Nitschke, J. R. Anion-induced reconstitution of a self-assembling system to express a chloride-binding $Co_{10}L_{15}$ pentagonal prism. *Nat. Chem.* **2012**, *4*, 751−765. (b) Saalfrank, R. W.; Burak, R.; Breit, A.; Stalke, D.; Herbst-Irmer, R.; Daub, J.; Porsch, M.; Bill, E.; Müther, M.; Trautwein, A. X. Mixed-valence, tetranuclear iron chelate complexes as endoreceptors: charge compensation through inclusion of cations. *Angew. Chem., Int. Ed. Engl.* **1994**, *33*, 1621−1623.
(21) Meng, W.; Clegg, J. K.; Thoburn, J. D.; Nitschke, J. R. Controlling the transmission of stereochemical information through space in terphenyl-edged Fe_4L_6 cages. *J. Am. Chem. Soc.* **2011**, *133*, 13652−13660.
(22) (a) Meng, W.; Ronson, T. K.; Nitschke, J. R. Symmetry breaking in self-assembled M_4L_6 cage complexes. *Proc. Natl. Acad. Sci. U. S. A.* **2013**, *110*, 10531−10535. (b) Clegg, J. K.; Cremers, J.; Hogben, A. J.; Breiner, B.; Smulders, M. M. J.; Thoburn, J. D.; Nitschke, J. R. A stimuli responsive system of self-assembled anion-binding $Fe_4L_6^{8+}$ cages. *Chem. Sci.* **2013**, *4*, 68−76.
(23) Que, L.; Tolman, W. B. Biologically inspired oxidation catalysis. *Nature* **2008**, *455*, 333−340.
(24) Rabion, A.; Chen, S.; Wang, J.; Buchanan, R. M.; Seris, J.-L.; Fish, R. H. Biomimetic oxidation studies. 9. Mechanistic aspects of the oxidation of alcohols with functional, active site methane mono-oxygenase enzyme models in aqueous solution. *J. Am. Chem. Soc.* **1995**, *117*, 12356−12357.
(25) MacFaul, P. A.; Arends, I. W. C. E.; Ingold, K. U.; Wayner, D. M. Oxygen activation by metal complexes and alkyl hydroperoxides. Applications of mechanistic probes to explore the role of alkoxyl radicals in alkane functionalization. *J. Chem. Soc., Perkin Trans. 2* **1997**, 135−145.
(26) McConnell, A. J.; Aitchison, C. M.; Grommet, A. B.; Nitschke, J. R. Subcomponent exchange transforms an $Fe^{II}_4L_4$ cage from high- to low-spin, switching guest release in a two-cage system. *J. Am. Chem. Soc.* **2017**, *139*, 6294−6297.

DOI: 10.1021/acs.inorgchem.7b01958
Inorg. Chem. XXXX, XXX, XXX−XXX